CHAPTER V
RESULTS AND DISCUSSIONS

5.1 Experimental Results

The instantaneous particle velocity is measured by using a CCD camera technique in a two-dimensional IIT gas-solids fluidized bed with the uniform inlet gas velocity of 33.55 cm/sec by pressure 30 psig at the compressor. The initial height of packed bed is 14.25 cm and CCD camera kept the data at height 14 cm for 5 positions: two left, center, and two right.

The experiment measures the axial and radial velocity at bed center height 14 cm. A view area is a 0.688 cm × 0.514 cm. The exposure time is 1/250 sec. The standard deviations of the radial and axial solids velocity for a bubble are 2.58 cm/sec and 3.86 cm/sec, respectively as shown in Figure 5.1.

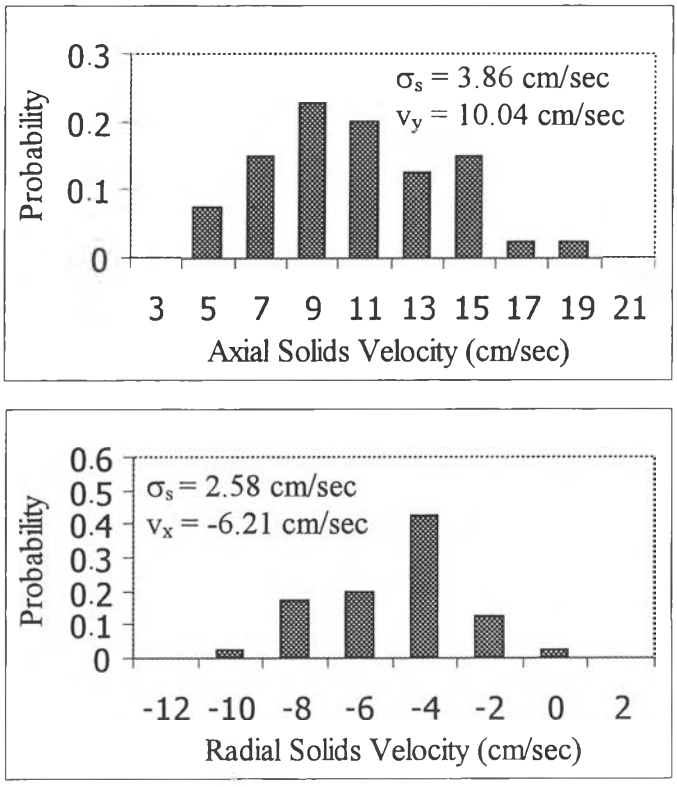

Figure 5.1 Histogram of axial and radial solids velocity for a bubble phase of 530 μ m glass beads at center region of the bed height of 14cm.

These histograms showed the probability of axial and radial velocity and their curves were similar to the normal distribution curve to check that these data were correct.

Figure 5.2 showed the time variances on hydrodynamic velocity of axial and radial directions calculated from Eq.(5.1), and Eq.(5.2). It showed the random oscillation of bubble with up-flow of particles at the center position. The axial velocity was higher than the radial velocity due to the fluid flow upward in axial direction.

Figure 5.3 showed the normal stresses of solids phase in x- and y-direction. They were derived from particle fluctuation velocity defined by instantaneous particle velocity (c(r,t)) minus hydrodynamic velocity of each frame, given by Eq. (5.3) and Eq(5.4). It could be seen from figure 5.3 that vertical normal stress ($<C_yC_y>$) was ten times higher than that of radial normal stress ($<C_xC_x>$). The granular temperature (θ) in Eq.(5.5), which was one third of the random particle kinetic energy, could be obtained from the normal stresses of particles.

$$u_j = \frac{1}{n_j}\sum_{i=1}^{n_j} c_{x_{i,j}} \tag{5.1}$$

$$v_j = \frac{1}{n_j}\sum_{i=1}^{n_j} c_{y_{i,j}} \tag{5.2}$$

$$\left\langle C_x C_x \right\rangle_j = \frac{1}{n_j}\sum_{i=1}^{n_j} [c_{x_{i,j}} - u_j][c_{x_{i,j}} - u_j] \tag{5.3}$$

$$\left\langle C_y C_y \right\rangle_j = \frac{1}{n_j}\sum_{i=1}^{n_j} [c_{y_{i,j}} - v_j][c_{y_{i,j}} - v_j] \tag{5.4}$$

$$\theta_{particle,j} = \frac{1}{3}\left[< C_x C_x >_j + < C_z C_z >_j + < C_y C_y >_j\right] \tag{5.5}$$

where $\theta_{particle,j}$ is the particle granular temperature. $c_{x_{i,k}}$ and $c_{y_{i,k}}$ are the radial and axial velocity of the i^{th} particle in the j^{th} frame, respectively. u_j and v_j are the average radial and axial velocity of the j^{th} frame. $\langle C_x C_x \rangle_j$, $\langle C_y C_y \rangle_j$ and $\langle C_z C_z \rangle_j$ are the normal stress in x-, y-, and z-direction, respectively. $\langle C_z C_z \rangle_j$ is approximately equaled to $\langle C_x C_x \rangle_j$. And n_j is the number of particle in the j^{th} frame.

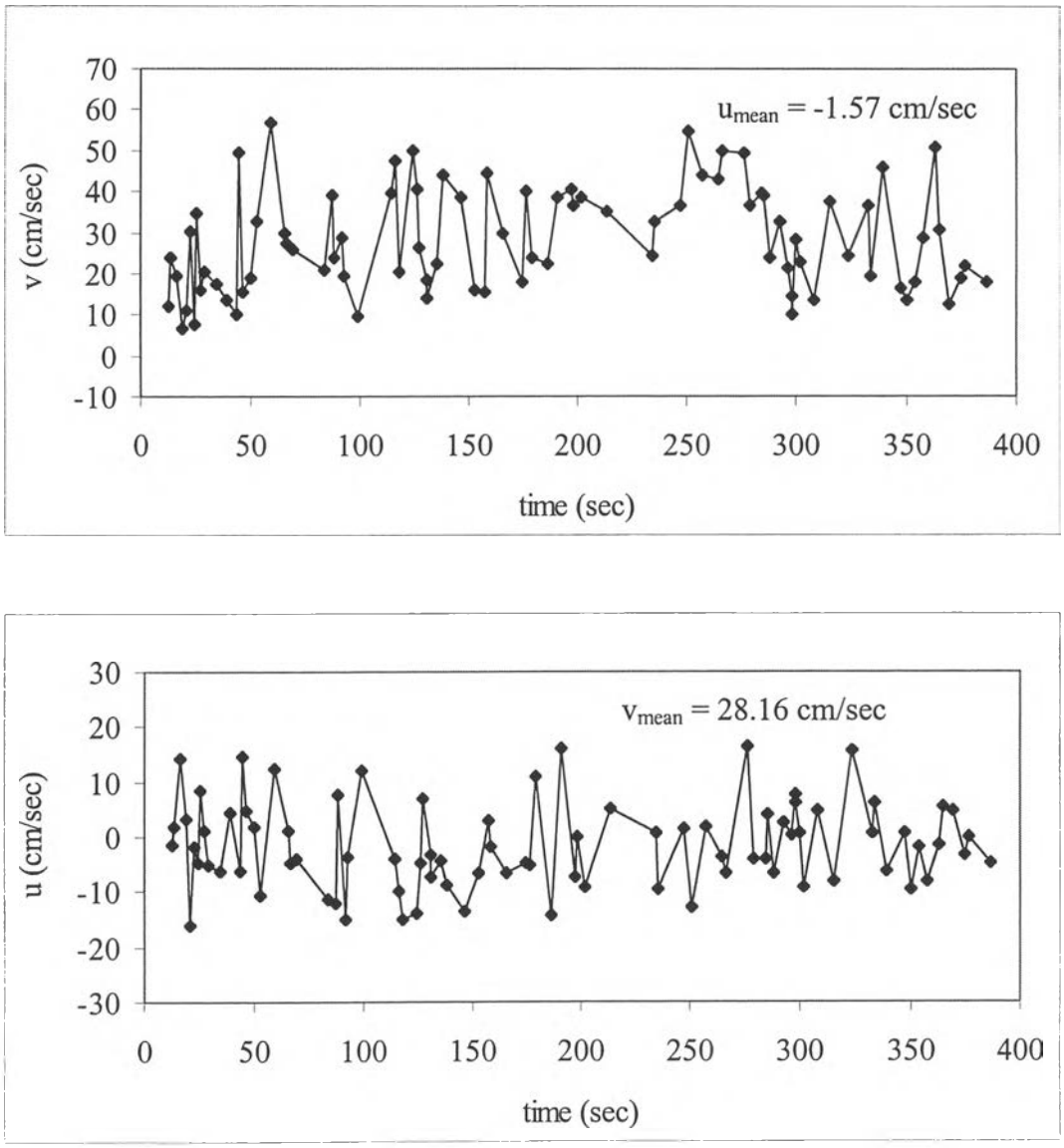

Figure 5.2 The time variances on hydrodynamic velocity of axial (v) and radial (u) direction obtained from each frame.

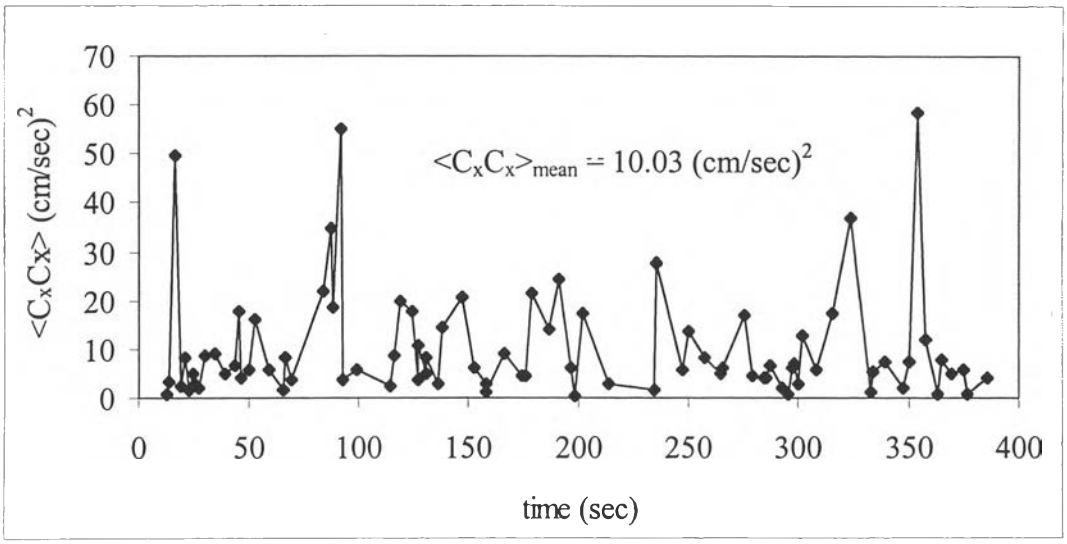

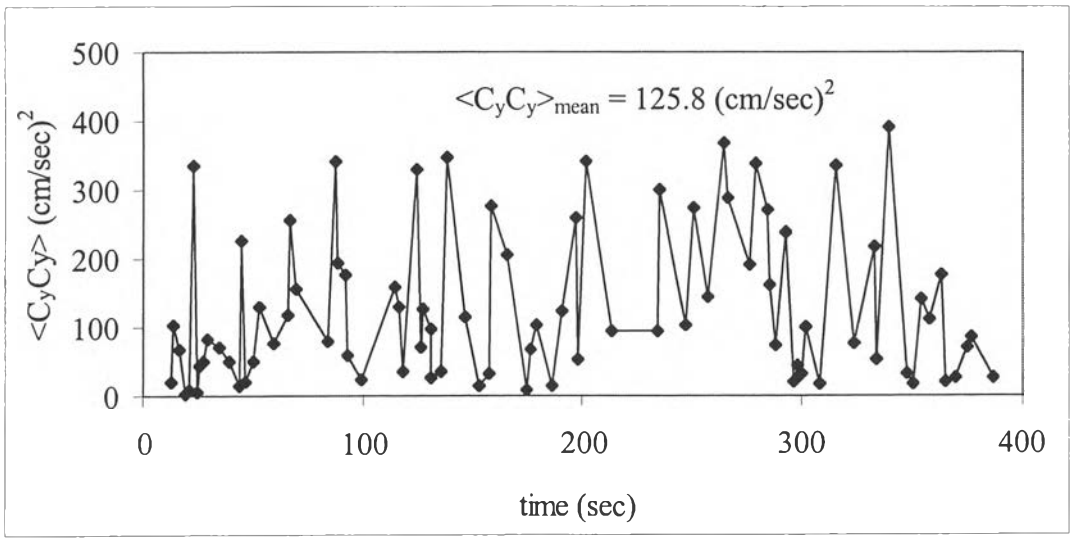

Figure 5.3 Normal stresses calculated from particle fluctuation velocity (C) defined by instantaneous particle velocity minus hydrodynamic velocity of each frame.

Hence, the particle granular temperature was a function of the time and space at given condition. The mean particle granular temperature was 48.62 cm^2/sec^2 for a bubble phase of 530 μm glass beads, which it calculated from Eq.(5.5). The unit of the granular temperature was cm^2/sec^2.

Figure 5.4 showed the shear stress of solids phase given by Eq.(5.6). The shear stress showed a low value of –8.17 cm^2/sec^2 at center position.

$$\langle C_x C_y \rangle_j = \frac{1}{n_j} \sum_{i=1}^{n_j} [c_{x_{i,j}} - u_j][c_{y_{i,j}} - v_j] \qquad (5.6)$$

where $\langle C_x C_y \rangle_j$ is the shear stress in the j^{th} frame.

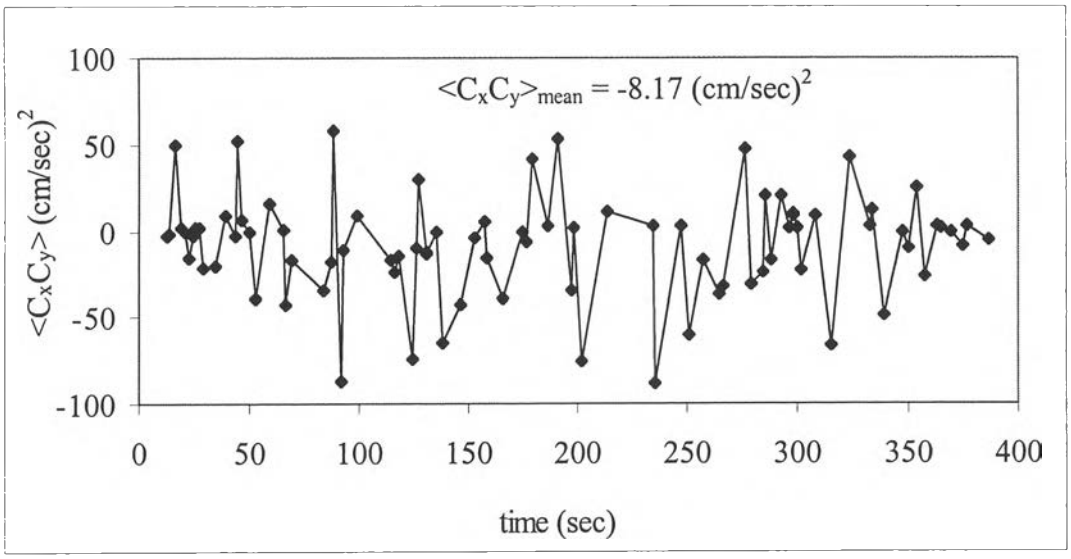

Figure 5.4 Shear stress calculated from particle fluctuation velocity (C) defined by instantaneous particle velocity minus hydrodynamic velocity of each frame.

Figure 5.5 showed the bubble diameter changed with time and the average bubble diameter obtained from the sum of every bubble diameter divided by the total number of data equaled to 5.0 cm.

$$D_B = 0.54(U - U_{mf})^{0.4}(h + 4\sqrt{A_0})^{0.8} / g^{0.2} \qquad (5.7)$$

where, D_B is the equivalent bubble diameter, U is the superficial gas velocity, U_{mf} is the minimum fluidization velocity, h is the height above the distributor, g is the gravitational acceleration and A_0 is the catchment area. $4\sqrt{A_o}$ is 0.03 m for porous plate gas distributor.

The bubble diameter from Davidson model, shown in Eq(5.7), equaled to 3.45 cm. The average bubble diameter from the experiment was higher than one from the Davidson model, because the experiment had the burst bubble at the height 14.0 cm. If the bubble diameters were measured at the height lower than that position, the bubble would not burst.

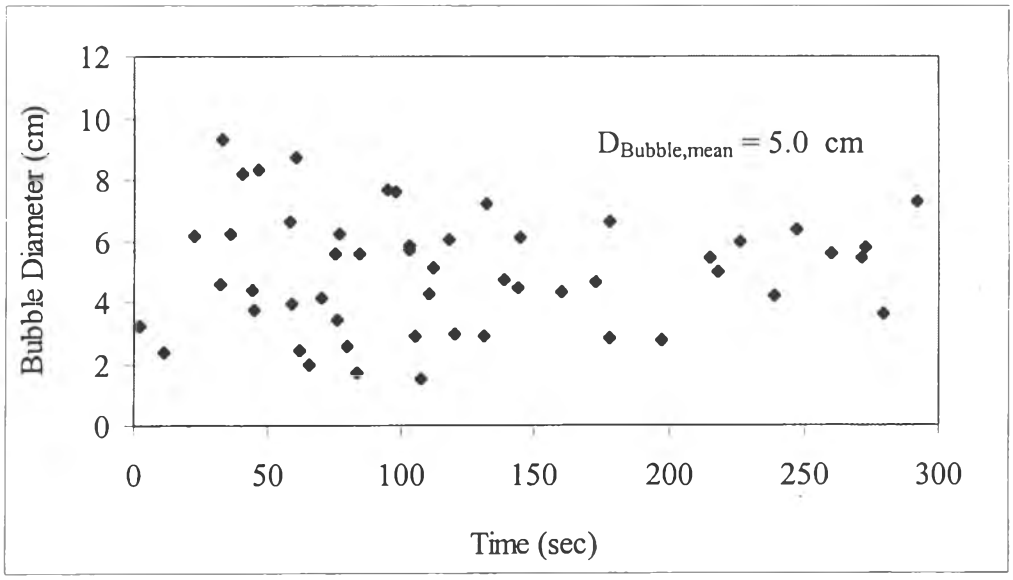

Figure 5.5 Equivalent bubble diameters obtained from snap shots of video camcorder.

Figure 5.6 showed the bubble rising velocity changed with time and the average bubble rising velocity obtained from the sum of every bubble rising velocity divided by the total number of data equaled to 36.99 cm/sec.

The relationship between bubble rising velocity (U_B) and bubble radius (r_B) had shown to be of the form (Grace, 1982) at gas velocities in excess of minimum

fluidization, as reviewed by Gidaspow (1994). The bubble velocity coefficient C was 2/3, which it was derived by Davies and Taylor (1950).

$$U_B = U - U_{mf} + C\sqrt{gr_B} \tag{5.8}$$

where, U_B is the bubble rising velocity, U is the superficial gas velocity, U_{mf} is the minimum fluidization velocity, r_B is the radius bubble, g is the gravitational acceleration and C is the bubble velocity coefficient equaled to 2/3.

The bubble rising velocity from Eq(5.8), equaled to 37.96 cm/sec, when the equation used the bubble radius from Davidson model. Because Eq.(5.8) needed to use the bubble radius, which was not burst. The average bubble rising velocity from the experiment was nearly one from Eq.(5.8).

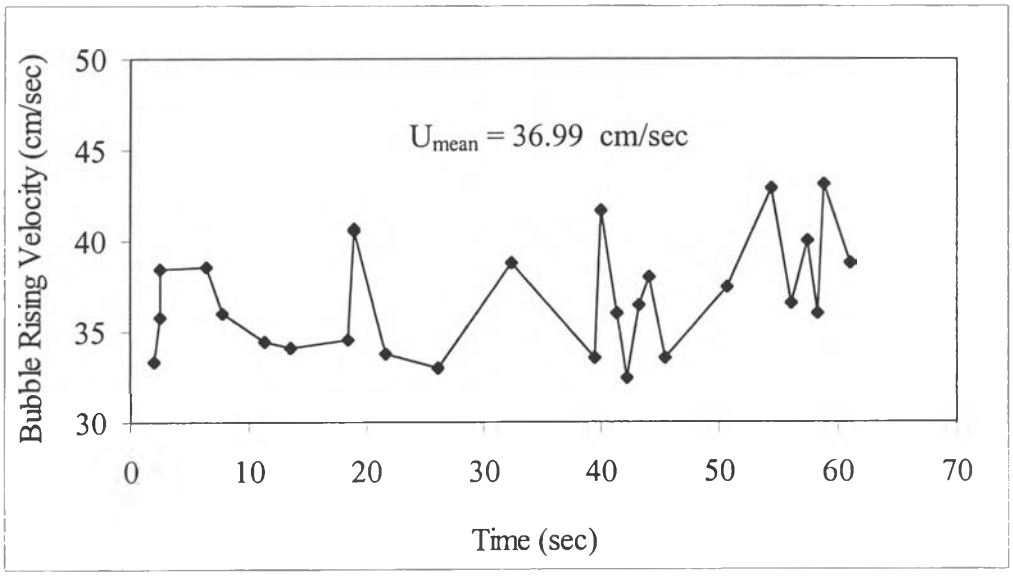

Figure 5.6 The time variance of bubble rising velocity.

Figures 5.7 and 5.8 showed the comparison of the granular temperatures measured by means of a CCD camera technique by using superficial velocity 58.7 cm/sec. From figure 5.7, the granular temperature of the bubble-like was more than that of the particle because the fluctuation of bubble-like velocity was more than that of particle velocity.

The particle granular temperatures ($\theta_{Particle,j}$) were calculated from particle normal stresses, Eq.(5.3) and (5.4), at each frame as previously shown in Eq.(5.5). It was the average of the particle granular temperature in each frame. Granular temperatures were weighted by the ratio of the number of picture of the emulsion phase and the bubble phase taken at same time.

The bubble-like granular temperatures ($\theta_{Bubble\text{-}like}$) were obtained from the variances of hydrodynamic velocity of solids phase shown in figure 5.2.

The normal stresses in x- and y-direction could find from Eq.(5.11) and Eq. (5.12), respectively. Eq.(5.9) and Eq.(5.10) takes in Eq.(5.11) and Eq.(5.12) to obtain the normal stresses in x- and y-direction. Those stresses were similar to the Reynolds stresses of single phase for a gas (Bird et. al, 1960). The bubble-like granular temperature was given by Eq.(5.13) with the same assumption used previously in Eq.(5.5).

$$\overline{u} = \frac{1}{N}\sum_{j=1}^{N} u_j \tag{5.9}$$

$$\overline{v} = \frac{1}{N}\sum_{j=1}^{N} v_j \tag{5.10}$$

$$\langle UU \rangle = \frac{1}{N}\sum_{j=1}^{N} \left(u_j - \overline{u}\right)\left(u_j - \overline{u}\right) \tag{5.11}$$

$$\langle VV \rangle = \frac{1}{N}\sum_{j=1}^{N} \left(v_j - \overline{v}\right)\left(v_j - \overline{v}\right) \tag{5.12}$$

$$\theta_{Bubble\text{-}like} = \frac{1}{3}\left[< UU > + < WW > + < VV >\right] = \frac{1}{3}\left[2 < UU > + < VV >\right] \tag{5.13}$$

where $\theta_{Bubble\text{-}like}$ is the bubble-like granular temperature. <UU>, <VV>, <WW> are normal stress in x-, y-, z-direction, respectively. <WW> is approximately equaled to <UU>. And $\overline{u}$ and $\overline{v}$ are the average radial and axial velocity.

The particle granular temperature was about 33 cm^2/sec^2 and the bubble-like granular temperature was about 65 cm^2/sec^2 shown in figure 5.7. The particle granular temperature due to particle oscillation was smaller than that of the bubble-like granular temperature at given experiment condition of the bubbling fluidized beds. When the conditions was changed, the particle granular temperature was found to be less than the bubble-like granular temperature as well.

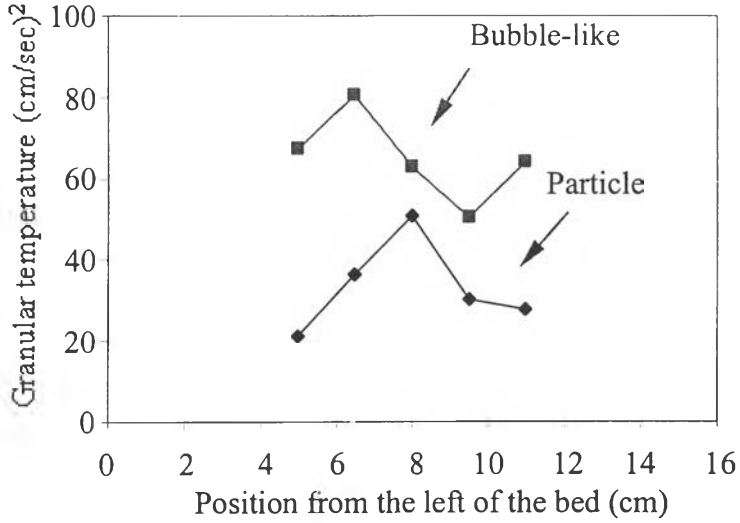

Figure 5.7 A comparison of measured particle and bubble-like granular temperatures for 530 μm glass beads at $U_0/U_{mf} = 2.5$.

From figure 5.8, the total granular temperature was a little higher than the bubble –like granular temperature. Therefore, the sum of the granular temperature between the bubble-like and particle was higher than the total granular temperature.

Total granular temperatures (θ_{Total}) were obtained from Eq.(5.16), the sum of all frames over time and velocity space given by Matonis et al. (2002) in a slurry bubble column, as shown in Figure 5.8. It used the average particle velocity of the system, as shown in Eq.(5.14) and Eq.(5.15).

$$c_{x0} = \frac{1}{\sum_{j=1}^{N} n_j} \sum_{j=1}^{N} \left[\sum_{i=1}^{n_j} c_{x_{i,j}} \right] \tag{5.14}$$

$$c_{y0} = \frac{1}{\sum_{j=1}^{N} n_j} \sum_{j=1}^{N} \left[\sum_{i=1}^{n_j} c_{y_{i,j}} \right] \tag{5.15}$$

$$\theta_{Total} = \frac{1}{3}\left[\frac{2}{\sum_{j=1}^{N} n_j} \sum_{j=1}^{N} \left[\sum_{i=1}^{n_j} (c_{x_{i,j}} - c_{x0})^2 \right] + \frac{1}{\sum_{j=1}^{N} n_j} \sum_{j=1}^{N} \left[\sum_{i=1}^{n_j} (c_{y_{i,j}} - c_{y0})^2 \right] \right] \tag{5.16}$$

where θ_{Total} is the total granular temperature. And c_{x0} and c_{y0} are the average particle velocity of the system in x- and y-direction, respectively.

The total granular temperature was about 75 cm^2/sec^2. The total granular temperature was about 20% lower value than sum of the granular temperature between the particle and the bubble-like shown in figure 5.8. They should be the same values statistically and might represent an error primarily due to insufficient frames in the velocity space.

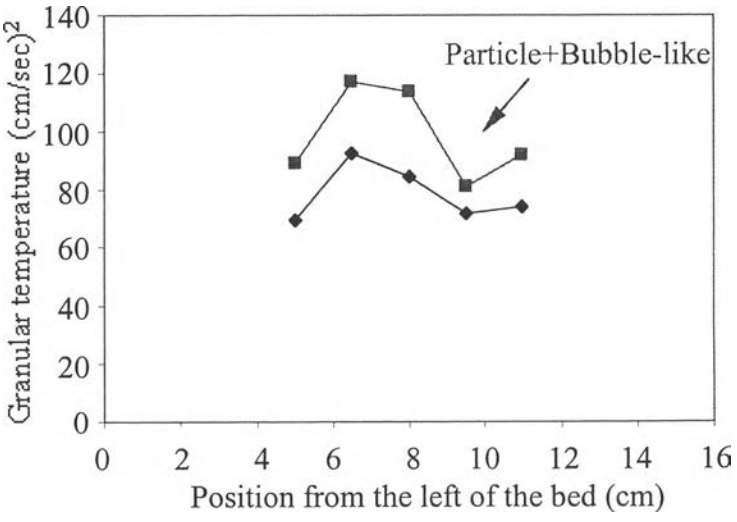

Figure 5.8 A comparison of the sum between particle and bubble-like granular temperature and velocity space for 530 μm glass beads at $U_0/U_{mf} = 2.5$.

5.2 Simulation Results

This simulation used model B in Gidaspow's book, in Multiphase Flow (1994). Figure 5.9 shows the solid volume fraction on this simulation.

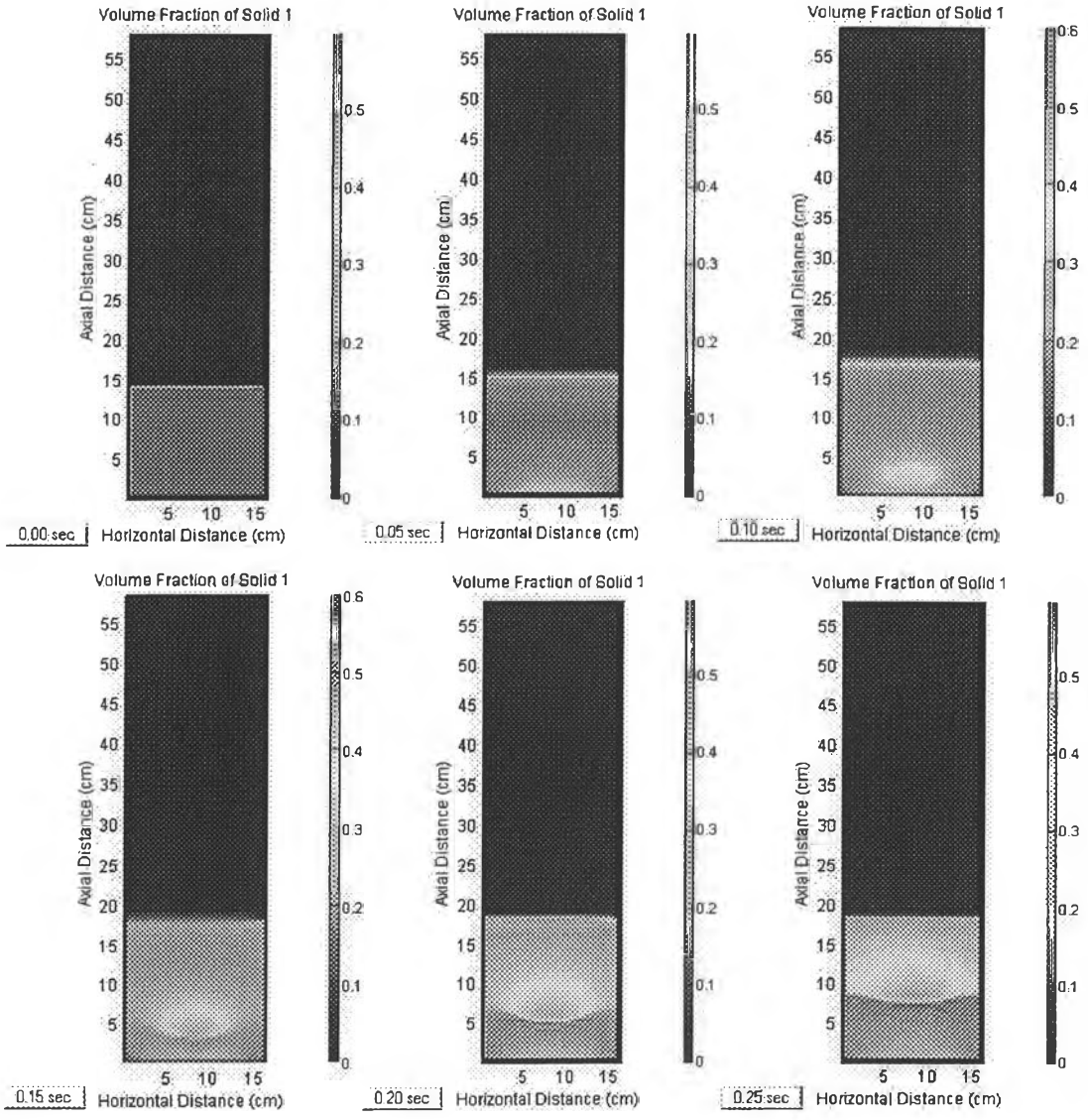

Figure 5.9 Simulation of glass bead 530 μm at air superficial velocity 68.5 cm/sec.

The Figure 5.9 shows the characteristic of the bubble in the simulation. At the initial time (0.00 second), the simulation bed did not have the inlet flow. Until the later time, the simulation bed would be the inlet flow and the bubble size expanded when the time increased.

Figure 5.10 shows the axial velocities at each height of the bed. Positive value represents the upward particles. On the other hand, negative value represents downward particles. At the both sides of the bed, the axial velocity increases with increasing bed height. However at the center of the bed, the velocity seems to be constant at any bed heights. From this figure, the axial velocity at center of bed (at 7.7 cm from the wall) is the lowest at bed height of 14.25 cm. It might be the effect of the burst bubble at the top of the bed.

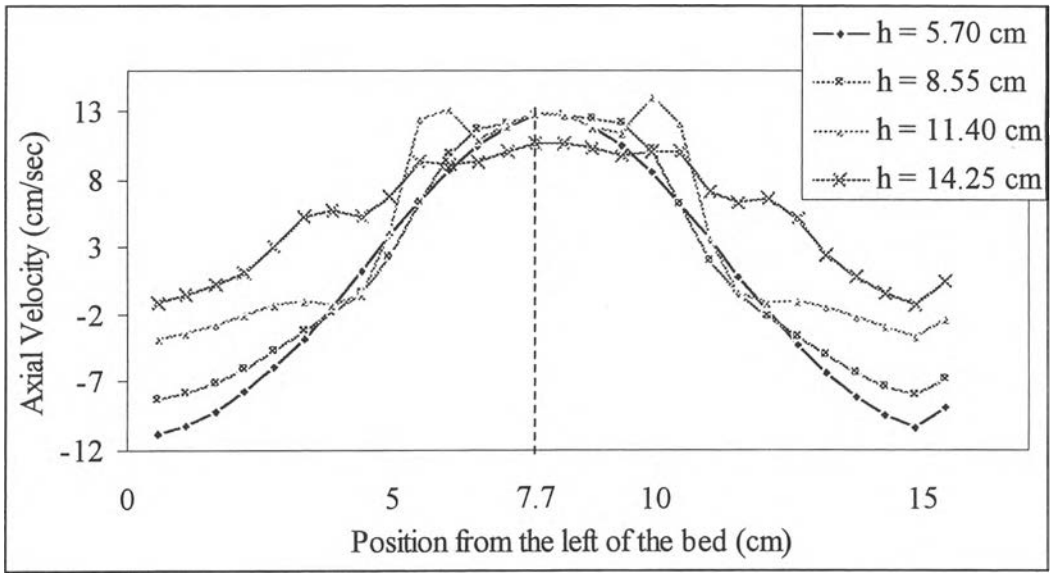

Figure 5.10 Axial velocity (cm/sec) on the simulation in each bed height.

Figure 5.11 shows the radial velocity at each bed height. Positive values of the radial velocity shows that the particles flowed from left to right. On the other hand, negative value shows that the particles flowed from right to left of the bed. The radial velocities at the both sides of the bed wall almost equaled to zero due to the no slip condition. The radial velocity at the center of the bed almost reached zero at every height because the bubble is generated at the center of the bed; therefore, the force balance in x-direction equals to zero. The figure also shows that at the lowest height of 5.70 cm, the particles near the wall move out from the wall. It might be the effect of the pressure from the wall acting on the particles.

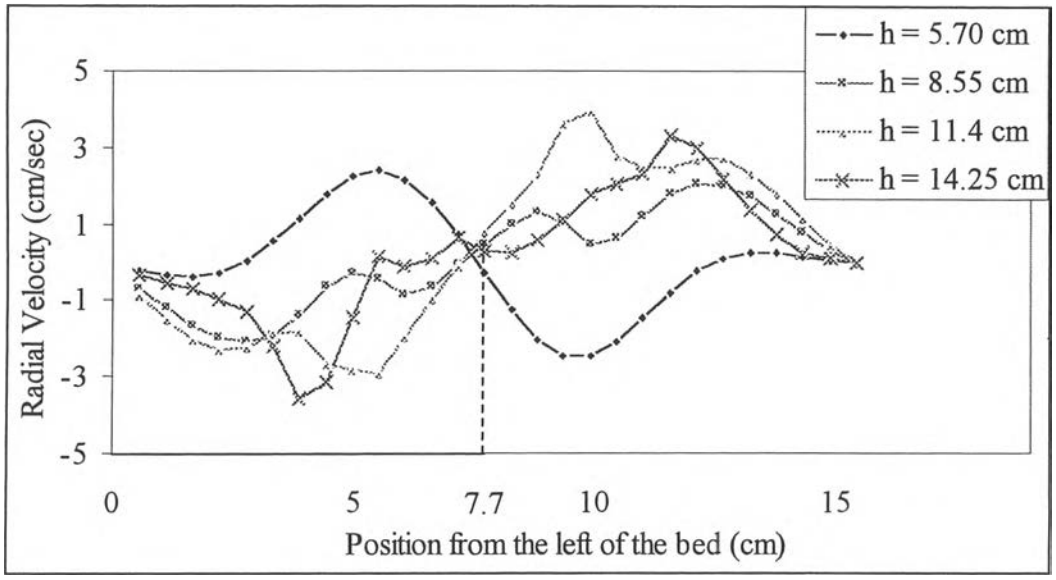

Figure 5.11 Radial velocity (cm/sec) on the simulation in each bed height.

Figure 5.12 shows the solid volume fraction at each bed height. As can be seen solid volume fraction varied from 0.30 to 0.40 at the height between 12 cm and 16 cm, which is the bubble region. At higher than 18 cm, solid volume fraction almost equaled to zero, which means that this region is the free board region.

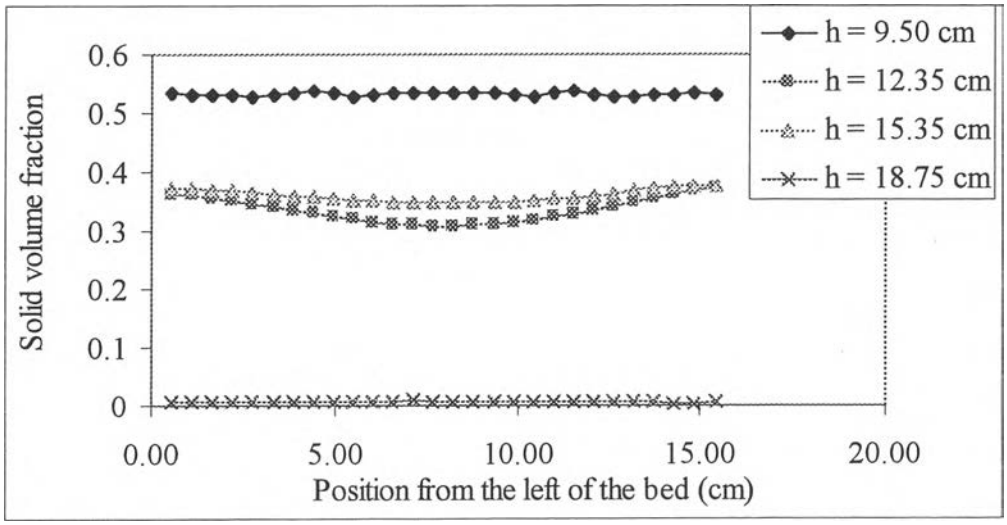

Figure 5.12 Solid volume fraction on the simulation in each bed height.

The results have small error when the simulation runs for short time.

5.3 Comparison of Experimental and Simulation Results

Figure 5.13 shows the comparison of axial and radial velocity from the simulation and the experiment. The particle velocity at the center is less than that of side of the wall, because the frequency of the bubble at the center is lower than that of the side of the wall. Therefore, the radial velocity at the center is lower than that at the side of the wall, as well. From the Figure 5.10, the errors in radial velocities for radial distance of 7.7, 9.2, and 10.7 cm are 1.49, 48.87, and 7.28 %, respectively. The errors in axial velocities for radial distance of 7.7, 9.2, and 10.7 cm are 13.21, 38.16, and 28.43 %, respectively.

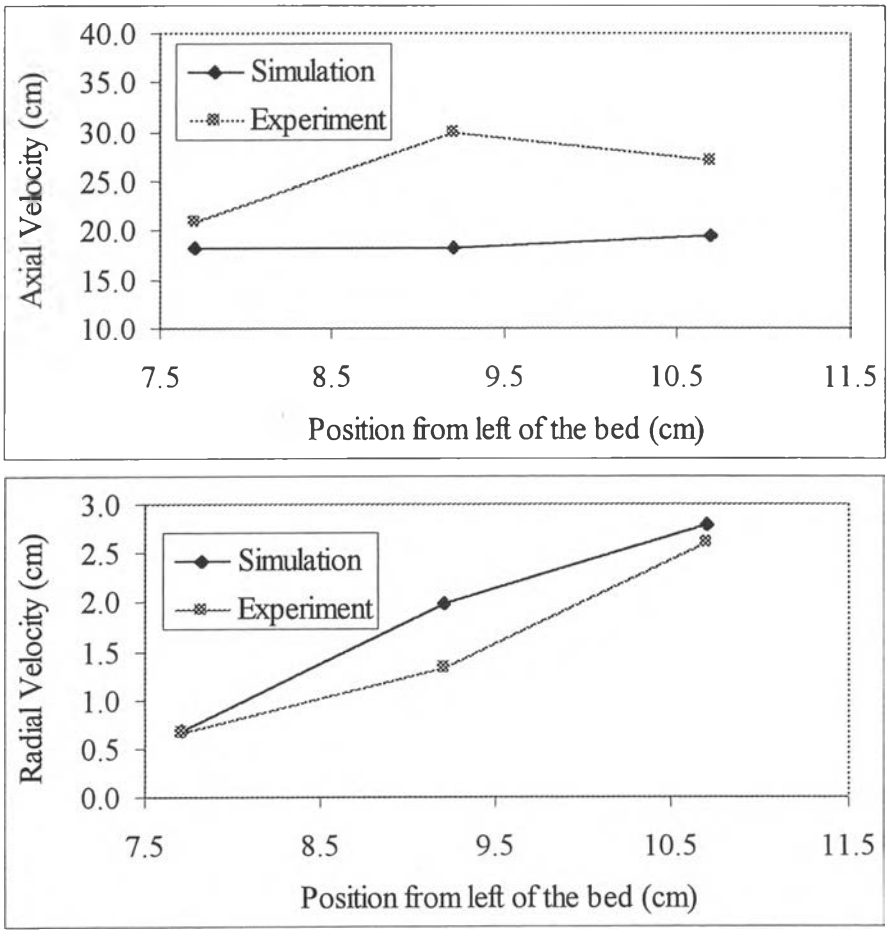

Figure 5.13 Comparison with axial and radial velocities of the results from the simulation and the experiment.

5.4 Discussion for the Experiment and Simulation

The data, which received from the experiment, can be plotted the axial velocity following Figure 5.14

The length inside the thin bed column is 15.4 cm, therefore, the position of the center from the left edge of this thin bed is 7.7 cm. All positions on the Figure 5.14 are 3.27, 5.13, 7.70, 10.27, and 12.13 cm, respectively. From the figure, the axial velocities of the glass beads decreased at the center region. After that it would increase again at the right of the thin bed column. Because the frequency of the bubble at center is lower than one at both sides of the wall as shown in Figure 5.15. The advantage of low superficial velocity is easily to obtain the bubble velocity.

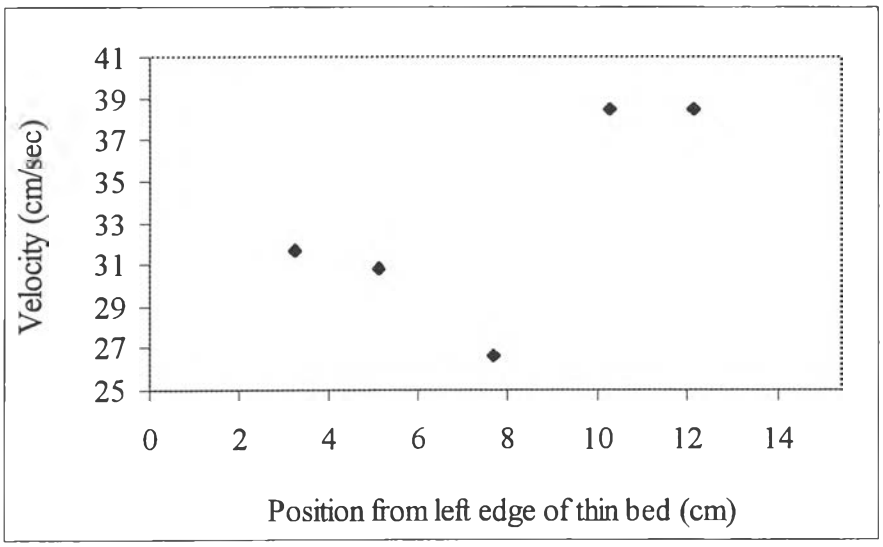

Figure 5.14 The relation between axial velocity and position.

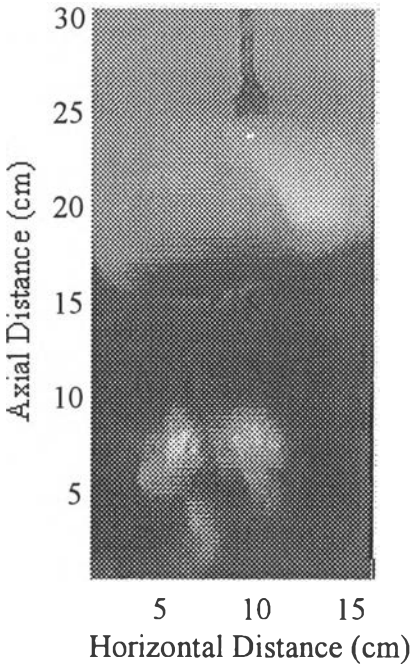

Figure 5.15 Experimental bubble captured by video camcorder.

The bubble velocity is found to be higher than the superficial velocity. Since the velocity of fluid in the thin bed, called interstitial velocity, is higher than the superficial velocity. The interstitial velocity equaled to the superficial velocity divided by porosity in the bed. In this case, the superficial velocity is 33.55 cm/sec and the bubble velocity is shown in Figure 5.6. The mean, minimum and maximum buble velocity are 36.99, 32.40, and 43.07 cm/second, respectively.

The errors of radial and axial velocities between the simulation and the experiment occurred from the simulation using finite differential instead of finite element. From Figure 5.10, when the velocities of the experiment increased, those of the simulation would increase as well.